Renewable Energy 249 (2025) 123085

Contents lists available at ScienceDirect

Renewable Energy

journal homepage: www.elsevier.com/locate/renene

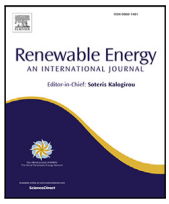

Optimizing energy production in PV systems: Comprehensive review of radiation models and key factors influencing power generation

Carlos Carbajosa [a,b,c,*], Sergio Marín-Coca [a,b,c], Miguel Gavira-Aladro [a,c], Alejandro Martínez-Cava [a,b,c]

[a] Universidad Politécnica de Madrid, Plaza Cardenal Cisneros, E-28040 Madrid, Spain
[b] Instituto Universitario de Microgravedad "Ignacio Da Riva" (IDR/UPM), Spain
[c] Escuela Técnica Superior de Ingeniería Aeronáutica y del Espacio (ETSIAE/UPM), Spain

ARTICLE INFO

Keywords:
Solar trackers
Energy production
Tilt angle
Geometric optimization

ABSTRACT

This paper presents a comprehensive framework for optimizing the orientation and spatial configuration of horizontally mounted photovoltaic (PV) panels to maximize annual energy yield. The proposed simplified deterministic mathematical model decouples factors influencing PV performance, enabling detailed analyses of geometric and utilization efficiencies. The framework applies to both fixed and solar-tracking systems, offering practical tools for determining optimal panel orientation based on latitude. Optimal dimensionless row spacing is also identified, although usually a balancing between energy production and practical concerns such as maintenance is required. The study highlights variability in existing radiation models and their coefficients, emphasizing the need for robust, location-independent optimization methods. It evaluates the effects of modeling assumptions, such as neglecting solar cell spacing in shading analyses, and identifies conditions under which these approximations remain valid. The sensitivity analysis carried out quantifies the impact of deviations from optimal configurations, illustrating the trade-offs between precise alignment and practical constraints. Validation against empirical data and literature shows consistent trends across diverse latitudes, demonstrating that the proposed mathematical model allows for the estimation of optimal angles in a universal manner, regardless of the specific characteristics of the studied location, beyond its latitude. By introducing a global efficiency metric, the framework integrates atmospheric, geometric, and system-level factors, providing a holistic approach to PV system design. These tools support early-stage planning for both standalone and industrial-scale solar installations, enhancing energy generation efficiency. Ultimately, this study offers a versatile and widely applicable methodology for optimizing PV system performance, contributing to more effective solar energy deployment worldwide.

1. Introduction

The global demand for energy has exhibited a consistently upward trend in recent decades, driven primarily by population growth and the increasing adoption of cooling technologies as a response to climate change [1]. Among all energy sectors, electricity has experienced the most significant growth. Projections from the International Energy Agency (IEA) estimate a 25% to 30% increase in electricity demand by 2030 compared to 2001 levels [1]. This growth is expected to be predominantly fueled by emerging economies, where population expansion and improved living standards are key driving factors. Renewable energy sources are anticipated to play a crucial role in these regions, promoting both energy security and equitable access to electricity [2].

Moreover, hybrid renewable energy systems are increasingly regarded as an essential strategy to address the economic and energy challenges faced by developing countries [3]. Currently, solar and wind energy contribute approximately 28% to global energy production (GEP), with projections suggesting an increase to 43% by 2030 [1]. Solar energy, in particular, holds immense potential; the solar energy reaching Earth in a single hour is sufficient to meet the global annual energy demand [4]. Solar energy can be harnessed through various technologies, including photovoltaic (PV) panels and solar thermal systems [5,6]. Among these, PV plants equipped with single-axis solar trackers have been identified as the most economically viable option for large-scale energy production [6]. These systems employ support

* Corresponding author at: Universidad Politécnica de Madrid, Plaza Cardenal Cisneros, E-28040 Madrid, Spain.
E-mail addresses: c.carbajosa@upm.es (C. Carbajosa), sergio.marin.coca@upm.es (S. Marín-Coca), miguel.gavira.aladro@alumnos.upm.es (M. Gavira-Aladro), alejandro.martinezcava@upm.es (A. Martínez-Cava).

https://doi.org/10.1016/j.renene.2025.123085
Received 22 January 2025; Received in revised form 21 March 2025; Accepted 7 April 2025
Available online 24 April 2025

structures that enable PV panels to follow the Sun's trajectory, thereby optimizing energy generation [7]. Such systems can significantly enhance energy output, with improvements ranging from 22% to 56% compared to fixed systems [8]. Photovoltaic energy generation is projected to grow exponentially, rising from 824 TWh in 2020 to 4011 TWh by 2030 [2].

The subsequent sections of this introduction explore key aspects pertinent to the modeling, design, and operation of photovoltaic (PV) solar panels. Specifically, the discussion focuses on the following topics:

1. Characterization of the total incident solar radiation on an inclined flat surface.
2. Characterization of the electrical performance and efficiency of PV solar cells.
3. Factors affecting the performance of PV panels.
4. Prior studies on orientation and spatial distribution optimization.
5. Paper contributions and structure.

1.1. Characterization of the total incident solar radiation on an inclined flat surface

Accurate characterization of solar radiation is essential for modeling the electrical production of solar energy systems, particularly PV solar panels. Over the years, numerous models have been developed to describe the factors influencing solar radiation and its distribution, with extraterrestrial radiation, atmospheric effects, and Earth's geometry being the most relevant ones. Within this context, the model proposed by Whillier [9] is particularly robust. It integrates the primary variables required for effective analysis while simplifying certain complex considerations that might limit practical applicability. Below, various radiation models are described, with justification provided for the selection of Whillier's model [9] in our work.

Historical models and their contributions

Initial studies on solar radiation date back to Angström [10], who proposed a model that highlighted the effects of factors such as cloud cover, fog presence, rain, as well as the critical role of diffuse radiation in high-latitude regions. The model proposes a linear relationship between daily total radiation Q, clear-day radiation Q_A, and the fraction of sunshine $S \in [0,1]$, expressed as $Q = Q_A(A_1 + A_2 S)$, where the fitted coefficients are $A_1 = 0.25$ and $A_2 = 0.75$. Despite its simplicity, regional adjustments were necessary for practical applications, as demonstrated by later refinements [11]. Black [12] introduced a dependency on the clearness index C instead of S, leading to more complex expressions such as $Q = Q_A(A_1 + A_2 C + A_3 C^2)$, which required experimental calibration for specific locations in order to determine the value of the coefficients A_1, A_2, and A_3. Further advancements by Swartman and Ogunlade [13] extended Angström's model by including relative air humidity R as an additional variable.

Moon [14] contributed a model emphasizing atmospheric physics, incorporating factors such as atmospheric absorption and scattering by gases and aerosols. While more comprehensive, this approach's complexity limited its application in practical engineering studies. The solar constant, with an average value of $SC = 1322$ W/m^2 (currently, the accepted value is $SC \simeq 1360$ W/m^2), became a key parameter, as variations caused by factors such as Earth–Sun distance, solar radiative behavior, and atmospheric scattering and absorption were typically less than 3.5%.

Significant progress was also achieved by Liu and Jordan [15], who decomposed radiation into direct and diffuse components and developed models for tilted surfaces incorporating ground-reflected radiation [16]. As the importance of radiation decomposition became evident, experimental models were developed in diverse regions, which emphasized the spatial and temporal variability of parameters.

Kondratyev [17] consolidated many of these developments, presenting detailed models for absorbed, scattered, and reflected radiation. Although his proposals offered a comprehensive characterization, the inherent complexity of certain atmospheric effects justified the use of proportionality constants in place of detailed modeling for practical applications.

Whillier's model

In contrast to earlier approaches, Whillier [9] proposed a model based on the atmospheric transmissivity factor $K = \dot{Q}/\dot{Q}_0$, where $\dot{Q}_0$ represents extraterrestrial irradiance and $\dot{Q}$ is the direct irradiance measured at the Earth's surface. This model offers several advantages over its predecessors:

1. *Simplicity and global applicability*: Unlike Angström's models and their derivatives, which require region-specific adjustments and knowledge of the percentage of sunshine S, Whillier's K factor provides a more universal description with typical values ranging from 0.3 to 0.75 depending on the location and time.
2. *Extraterrestrial irradiance calculation*: Extraterrestrial irradiance, $\dot{Q}_0$, can be derived from a quasi-steady-state isotropic radiation model. Using this approach, extraterrestrial irradiance is expressed as:

$$\dot{Q}_0(t) = \sigma T_{Sun}^4 \left[\frac{R_{Sun}}{R(t)}\right]^2, \tag{1}$$

   where $\sigma = 5.67 \cdot 10^{-8}$ W/m^2 K^4 is the Stefan–Boltzmann constant, $T_{Sun} = 5772$ K is the Sun's equivalent blackbody temperature, $R_{Sun} = 6.96 \cdot 10^8$ m is the solar radius, and $R(t)$ is the time evolution of the Earth–Sun distance. This method enables highly accurate computation of $\dot{Q}_0$.
3. *Astrodynamical considerations*: To account for Earth's orbital variations, its Keplerian motion can be considered, assuming both bodies are perfect spheres and neglecting third-body influences. Consequently, the Earth–Sun distance $R(t)$ is expressed as:

$$R(t) = \frac{SMA\left(1 - ECC^2\right)}{1 + ECC\cos(\Omega(t))}, \tag{2}$$

   where $SMA \simeq 1.4960 \cdot 10^{11}$ m is the orbital semi-major axis, $ECC \simeq 0.0167$ is the orbital eccentricity, and $\Omega(t) \approx \Omega_{Sun,0} + \omega_{Sun} t + 2\pi - AOP$ represents the angular position. Here, $\Omega_{Sun,0}$ is the reference angular position, and $\omega_{Sun} = 2\pi/(365.25 \cdot 24 \cdot 3600)$ rad/s is the mean angular velocity of Earth's orbital motion. This formulation ensures precise representation of seasonal variations in solar radiation, except for second-order errors in ECC, since it has been assumed that the mean and true anomalies are approximately equal (due to the low eccentricity of the Earth's orbit).
4. *Adaptability to local conditions*: Although Whillier's model assumes certain idealizations, such as the absence of clouds and exclusively direct radiation, it can be extended to include local effects such as albedo and diffuse radiation in combination with complementary models.

The factor K also incorporates the atmospheric impact on radiation transmission, facilitating its application in studies where atmospheric influence is significant, without requiring detailed characterization of components such as humidity or turbidity. In this paper, it is assumed that K encompasses all factors that, for a given location, cause the experimentally observed annual average solar radiation to deviate from the corresponding extraterrestrial radiation.

Decomposition of solar radiation into its components

The decomposition of solar radiation into its direct and diffuse components is critical for numerous studies in solar energy, as these components influence the design and performance of PV and thermal systems in distinct ways. While there has been a significant increase in the measurement of total radiation, it is often essential to independently assess these components to achieve accurate estimations [18].

Among prominent approaches, Hay [19] proposed a model incorporating multiple reflections to calculate diffuse radiation, accounting for the region's albedo and backscattering (*i.e.*, radiation reflected from the ground back towards the clouds). Similarly, Orgill and Hollands [20] developed a piecewise linear correlation between K_d (the ratio of diffuse to total radiation) and K_T (the ratio of total to extraterrestrial radiation).

Klein [21] compared alternative methods for deriving diffuse radiation from total radiation, demonstrating comparable performance. However, studies like those by Ruth and Chant [22] revealed that the Liu and Jordan model [15], which estimates diffuse radiation based on total radiation, lacks universality as its accuracy varies with latitude. In line with this, Bruno [23] adapted the Liu and Jordan model for application in West Germany, emphasizing the need to tailor model parameters to specific geographical contexts.

Other approaches include corrections by Suckling and Hay [24] to estimate direct, diffuse, and total radiation under partially cloudy skies using parameters such as cloud cover and sunshine duration. Reindl et al. [25] developed correlations based on data from the United States and Europe, while Erbs et al. [26] and Spencer [27] explored specific correlations and methods to estimate diffuse radiation in diverse geographic locations. Finally, due to the complexity of obtaining precise values of the clearness index and diffuse fraction, Hollands and Huget [28] argued for treating them as random variables, proposing probabilistic models to describe their distribution.

Advances in solar radiation models

Recent years have seen substantial advancements in solar radiation models, incorporating climatic, geographic, and atmospheric variables to improve accuracy. Hay [29] introduced a comprehensive approach for calculating daily radiation, considering multiple reflections between the Earth's surface and the atmosphere as well as albedo. This model allows estimation of direct, diffuse, and reflected radiation on inclined surfaces and highlights that the relationships among radiation components remain proportional under constant sunlight fraction and albedo conditions. Furthermore, Bendt et al. [30] introduced a clearness index based on the fraction of time it remains below certain values, useful for evaluating climatic patterns.

Gueymard [31] described various models with differing input data and behaviors. Despite their complexity, for a specific location it can generally be assumed that global radiation is proportional to extraterrestrial radiation, with the proportionality constant depending on the location. Input data for these models include site-specific pressure and temperature, reduced ozone path length, precipitable water, turbidity parameters, aerosol single-scattering albedo, aerosol transparency coefficient, aerosol optical thickness at specific wavelengths, clearness number, visibility, and average zonal albedo. Davies et al. [32] examined global radiation under clear and cloudy skies, accounting for effects such as absorption, diffusion, reflection, precipitation, and cloud properties across different atmospheric layers.

In this context, advanced studies have also introduced models to treat diffuse radiation with greater precision. For instance, Hay [19] and Bruno [23] emphasized the radial behavior of diffuse radiation and its interaction with ground-reflected radiation, highlighting implications for inclined solar systems. The total radiation, comprising direct, diffuse, and reflected components, tends to follow an effective direction similar to direct radiation due to compensation between diffuse and reflected components. Additionally, Reindl et al. [25] and Hollands and Huget [28] addressed seasonal variability and the uncertainty associated with cloudiness indices, stressing the importance of adapting models to local data.

Nevertheless, Norris [33] concluded that predicting solar radiation from cloud cover data remains challenging due to the variability in transmitted radiation intensity and the potential contribution of reflected radiation.

Summary and assumptions

In summary, ongoing development in solar radiation models has enabled integration of complex variables such as cloud effects, atmospheric properties, and local terrain characteristics, improving the precision and adaptability of radiation estimates under diverse climatic and geographic conditions. However, the complexity and variability of model coefficients with respect to location and time often favor simplified linear models with constant coefficients. These coefficients can be adjusted based on site-specific data collected over time through *in situ* experiments.

In this study, we assume that total local irradiance can be expressed as $\dot{Q}_T(t) = K_T \dot{Q}_0(t)$, where $\dot{Q}_0(t)$ represents extraterrestrial irradiance as given by Eq. (1), and the coefficient K_T accounts for all effects included in Whillier's model [34], along with contributions from diffuse and reflected radiation (in addition to direct radiation) to total radiation. It is further assumed that total radiation is incident in the direction of direct radiation, which is determined for each location based on the relative position between the Sun and Earth.

1.2. Characterization of the electrical performance and efficiency of PV solar cells

Once the solar irradiance incident on a surface containing a PV solar cell is determined, various models can describe the electrical performance of the cell in terms of energy production. These models depend on the internal structure of the PV cell and typically involve modeling through the use of electronic components such as diodes and resistors [35]. In general, the current of the electrical signal produced by the cell depend on the solar irradiance, output voltage and temperature, requiring specific coefficients to be calibrated for each individual cell. A range of models exists, from simple approximations to highly detailed simulations [35,36].

A common practice is to relate the electrical power produced by the cell to its maximum achievable power through the fill factor, FF. Furthermore, it is important to relate the maximum power output of the cell under a given irradiance to the irradiance itself. The combination of these two concepts leads to the cell efficiency η_{cell}, which quantifies the ratio of the power generated by the PV cell to the incident solar power on its surface [37].

Over the years, the efficiency of PV cells has increased significantly, with considerable variation between different technologies [38]. Currently, efficiency values range from approximately 15% for inorganic CZTSSe cells to nearly 50% for monolithic cells with four or more junctions. Notably, the FhG-ISE cell holds the record for the highest efficiency to date, achieving 47.6% [39].

1.3. Factors affecting the performance of PV panels

While knowing the total incident solar irradiance and cell efficiency is crucial for determining the electrical energy output of a PV cell, additional factors influence energy production when cells are integrated into solar panels and deployed across specific terrains.

One such factor involves solar tracking systems, which optimize the orientation of PV panels to maximize solar capture. Solar trackers can be categorized into single-axis and dual-axis systems, as well as passive and active systems [8]. Single-axis trackers rotate around a single axis, while dual-axis trackers offer more precise alignment by rotating along two axes. Passive trackers utilize the Sun's thermal energy to adjust panel orientation, whereas active trackers rely on sensors and motors for positioning [8].

Beyond solar tracking systems, several other factors play a crucial role in optimizing the performance of PV systems [7,40]:

1. *Kelly cosine effect*: When light strikes a solar panel, the perpendicular component of the incident light deviates slightly from a cosine function as the angle of incidence changes. This phenomenon, known as the Kelly cosine effect, follows a curve that diverges from the cosine function at angles greater than approximately 60° from the panel normal. Beyond roughly 85°, energy capture drops to zero [41]. However, the impact of this effect is minor and is therefore not considered in this study.

2. *Maximum power point operation*: The use of maximum power point tracking (MPPT) controllers ensures that PV panels operate at their highest efficiency [7]. This paper assumes that the solar panels under consideration are equipped with MPPT technology.
3. *Operating temperature*: The electrical output of PV systems decreases as operating temperature increases [42]. Technologies for cooling PV panels include both active methods, which consume electrical power, and passive methods, which do not [43]. While many cooling techniques use wind for convective heat dissipation, concerns about aeroelastic effects on solar trackers have grown, as such effects can lead to catastrophic failures [44,45]. Given the challenges in forecasting ambient temperature and wind at specific sites, this study assumes that the cell efficiency values used already incorporate these and other environmental effects as averaged factors for the given location.
4. *Packing factor*: The packing factor, $\eta_{pack} = A_{cell}/A_{panel}$, is the ratio of the area occupied by PV cells, A_{cell}, to the total panel area, A_{panel} [40]. Reducing the packing factor decreases the solar radiation captured by the cells but also improves thermal dissipation due to greater spacing, thereby enhancing efficiency. This trade-off creates an optimal packing factor for each PV cell technology and environmental condition.
5. *Shading*: The presence of obstacles or rows of panels can create shadows that significantly reduce electrical output [46–48]. When a PV cell becomes shaded, it ceases production entirely. This paper incorporates a model that accounts for the internal distribution of PV cells and their behavior under shading. It demonstrates that when the distances between cells and their dimensions are small relative to the panel dimensions, the shading effect can be approximated in a continuous manner.
6. *Dust, dirt, and cleaning techniques*: Dust and dirt reduce the irradiance reaching the cells and increase local temperatures due to absorbed solar radiation, thus decreasing cell efficiency. To address this, various cleaning systems (both active and passive) have been developed [49]. In this paper, routine maintenance is assumed to mitigate these effects, allowing dust and dirt to be neglected.
7. *Degradation*: Over time, PV cells degrade, resulting in efficiency losses. On average, this degradation is approximately 1% annually over the first 10 years [50]. Since this effect is minor over a single year, it is not considered in the optimization of panel orientation and spacing in this study.

1.4. Prior studies on orientation and spatial distribution optimization

Early studies on the optimization of fixed solar panel orientation incorporated the effects of different types of radiation and temperature. These studies required detailed modeling of numerous parameters specific to each location [51]. Optimal tilt angles could be derived for monthly or annual periods, depending on the temporal scope of the optimization, leading to various models for determining the optimal tilt angle over a given time frame [52].

In recent years, the number of studies characterizing site-specific conditions and determining optimal PV panel orientations has grown significantly [53,54]. Furthermore, advancements in solar radiation modeling have emerged, with isotropic and anisotropic models being the most prominent [55,56]. Within these two broad categories, researchers propose various methods for adjusting coefficients, complicating the universal application of results [55,56]. Several studies in the literature compile information on the optimal tilt angles of solar panels. The 2013 study by Darhmaoui and Lahjouji [54] proposes a method for determining the optimal tilt angle that maximizes energy production in various Mediterranean countries. Similarly, the 2017 study by Hafez et al. [56] presents a comprehensive literature review, compiling models proposed by different authors to determine the optimal tilt angle based on various parameters, including site latitude. In addition, the 2018 study by Jacobson and Jadhav [57] calculates optimal tilt angles for different countries using the PVWatts software developed by the National Renewable Energy Laboratory. The results available in the literature and synthesized in these three studies are used in this paper to validate the model developed herein.

Although solar irradiance varies significantly by location, factors such as the Earth–Sun distance and latitude have a greater effect on irradiation than local atmospheric conditions over time and space [58]. While these astronomical effects can be accurately predicted for the future, atmospheric effects, including cloud cover, are harder to forecast. Despite advances in deep learning techniques, reliable long-term atmospheric predictions remain elusive, with current models being limited to short-term forecasting [59].

The need for simple, fast methods during early design phases, combined with the difficulty of characterizing and predicting site-specific conditions, highlights the importance of developing a straightforward model applicable to generic locations. Such a model should estimate the optimal panel orientation and evaluate the sensitivity of performance to deviations from this optimal orientation due to other constraints [60].

1.5. Paper contributions and structure

As described in the preceding paragraphs, there are currently numerous radiation models, each exhibiting significant variability depending on the selected site. Moreover, the coefficients involved in these models also demonstrate substantial variability over time, making future predictions challenging. Consequently, while there are many studies aimed at determining the optimal orientation for specific locations using these models (as evidenced by the research papers and reviews conducted by Darhmaoui and Lahjouji [54], Hafez et al. [56], and Jacobson and Jadhav [57]), the results show considerable variability between locations, and the optimal orientations for the same site may vary from one year to another. Additionally, the substantial volume of research focused on orientation optimization contrasts with the relatively limited literature addressing the analysis of row spacing from the perspective of maximizing energy production. Given the variability of available models, it is important to assess the sensitivity of optimal configurations to deviations in PV panel orientation from the calculated optimum and to variations in row spacing in systems with multiple solar tracking rows. Furthermore, existing studies often focus on partial optimizations or specific aspects, lacking a comprehensive perspective on the integrated performance of photovoltaic energy systems.

This paper aims to address these gaps by providing a holistic perspective on the factors influencing the electricity production of both fixed solar panels and single-axis and dual-axis solar trackers. In this regard, the study seeks to develop a universal, simplified deterministic mathematical model that accounts for all aspects affecting energy production through fixed solar panels, and single-axis and dual-axis solar trackers, enabling the estimation of energy production for both photovoltaic panels and solar trackers. Based on this holistic model, the goal is to identify the values of key parameters influencing energy production that maximize the annual energy output of fixed solar panels and solar trackers. Additionally, throughout the paper, a series of efficiency metrics are introduced, considering various aspects of performance, and a global efficiency metric is defined to estimate the performance of both individual-scale photovoltaic panels and industrial-scale photovoltaic plants. By optimizing the annual average global efficiency, the optimal panel orientations as a function of latitude are determined and expressed as a fifth-degree polynomial. The developed simplified deterministic mathematical model also allows for the evaluation of the influence and sensitivity of electrical production to various factors, including average atmospheric conditions, photovoltaic cell efficiency and packing factors, Earth–Sun distance, solar tracking algorithms (in the case of trackers), and row spacing. The proposed simplified model is robust, and the optimal configurations derived from it are independent

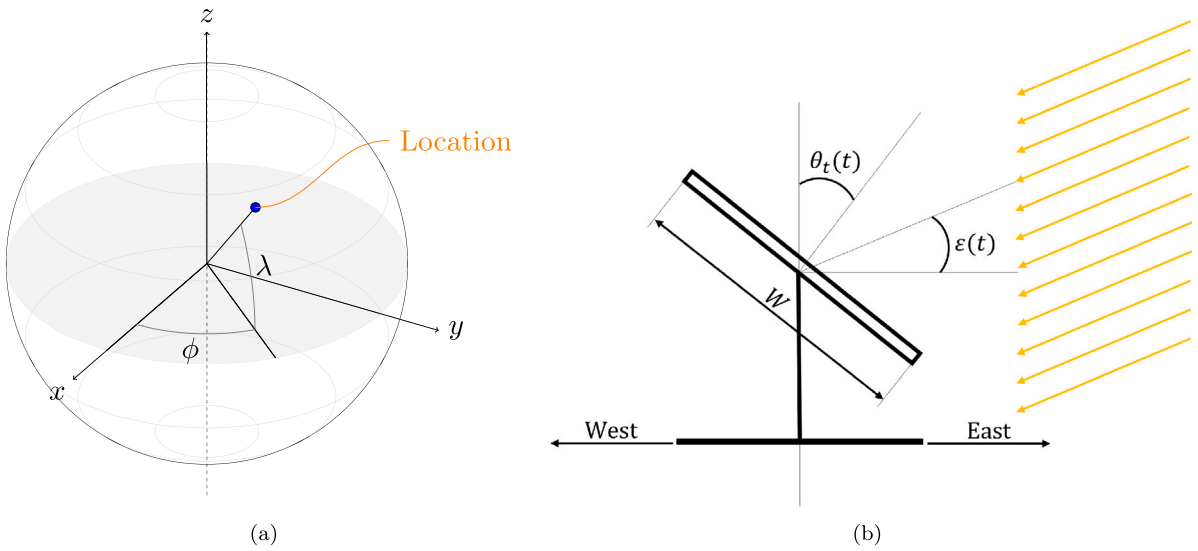

Fig. 1. Diagram illustrating: (a) the spherical coordinates (longitude, λ, and latitude, ϕ) of the selected location; and (b) the solar elevation angle (measured from the east), $\varepsilon(t)$, along with the seat angle of the solar panel or horizontally mounted solar tracker in the east–west direction (measured as positive towards the east), $\theta_t(t)$.

of the characteristics of the selected site. Furthermore, the optimal configurations obtained with this model are compared with other results from the literature, revealing consistent trends.

This paper is organized as follows: Section 1 provides a comprehensive overview of the factors affecting electricity production using PV panels, including modeling and design considerations. Section 2 introduces a simplified mathematical model for estimating the electrical output of PV systems, encompassing fixed panels as well as single-axis and dual-axis solar trackers. This model provides a holistic view of the factors influencing electrical energy generation in industrial PV plants. Section 3 details the geometric optimization of panel orientation and row spacing to maximize annual energy capture, along with a sensitivity analysis of energy production with respect to optimal configurations. Finally, the conclusions are summarized in Section 4.

2. Mathematical formulation

The analysis considers a specified number, N, of horizontally mounted solar panel rows installed at a location characterized by its longitude, λ, and latitude, ϕ (see Fig. 1-(a)). Each solar panel is defined by its chord (W) and span (L), with the panels oriented such that their span aligns along the north–south axis (see Fig. 2), and their chord extends along the east–west axis (see Fig. 1-(b)). The configuration assumes that there is one panel per row, with area $L \cdot W$ meaning the total number of panels is also equal to N. Additionally, the solar panels and solar trackers considered form, at any given moment in time, two angles with the local vertical: the seat, θ, and the tilt, β, angles. The former is the angle they form in the east–west direction with the local vertical, measured positively towards the east, as shown in Fig. 1-(b); while the latter is the angle they form in the north–south direction with the local vertical, measured positively towards the north, as depicted in Fig. 2.

The analysis also accounts for the potential shading of the solar panel by obstacles that may obstruct sunlight. To evaluate this, the solar elevation angle, ε, is considered (see Fig. 1-(b)). This angle represents the inclination of the Sun's direction relative to the local horizontal plane. The solar elevation angle ranges from 0 radians when the Sun is at the eastern horizon to π radians when it reaches the western horizon. The panel is illuminated only within a defined range of solar elevation angles, bounded by ε_{min} and ε_{max}, such that $\varepsilon \in [\varepsilon_{min}, \varepsilon_{max}]$.

Furthermore, four different types of solar PV systems are distinguished: fixed solar panels, which keep constant their orientation with respect to the ground; single-axis east–west solar trackers, which follow the Sun in its daily east–west movement; single-axis north–south solar trackers, which follow the Sun in its yearly north–south movement; and dual-axis solar trackers, which follow the Sun both in its east–west movement and its north–south movement throughout the year. In the case of fixed solar panels, a single panel is considered, *i.e.*, $N = 1$, because it is assumed that there will be no shading between panels, so if there are multiple rows, the production is equivalent to having a single row with the same area and orientation. For single-axis east–west trackers, it is considered that the rotation axes of all of them are separated by the same distance, D.

2.1. Projections of incident solar power

Since only the incident solar radiation perpendicular to the PV panel intervenes in the electric power generation, it required knowing the angles formed between the solar vector and the normal direction of the PV panel. For this purpose, the expressions that allow determining the direction of the Sun as a function of the time instant, t, shall be given. The unit vector in the direction connecting the center of the Earth with the Sun is given by its coordinates in the inertial reference system with origin at the center of the Earth; the x-axis pointing towards Aries; the z-axis perpendicular to the equatorial plane and pointing north; and the y-axis forming a right-handed triad; which are:

$$\vec{u}_{Sun}(t) = \left\{ \begin{matrix} \cos\left(\Omega_{Sun,0} + \omega_{Sun} t\right) \\ \sin(\epsilon)\sin\left(\Omega_{Sun,0} + \omega_{Sun} t\right) \end{matrix} , \cos(\epsilon)\sin\left(\Omega_{Sun,0} + \omega_{Sun} t\right) \right\}, \quad (3)$$

where $\epsilon \simeq 23.44°$ represents the angle between the plane of the ecliptic and the plane of the Earth's equator.

On the other hand, it is convenient to define a triad linked to the point (λ, ϕ) being analyzed. This triad is taken so that the radial unit vector, $\vec{u}_r$, points in the radial direction; the azimuthal unit vector, $\vec{u}_\lambda$, is tangent to the parallel corresponding to the considered latitude, and points positively east; and the polar unit vector, $\vec{u}_\phi$, completes the right-handed triad, so that it is tangent to the corresponding meridian, and points north. Thus, for a given point, determined by its longitude and latitude, (λ, ϕ), the coordinates of the previous unit vectors in the described inertial triad are:

$$\vec{u}_r(t) = \left\{\cos(\phi)\cos\left(\lambda + \omega_{Earth} t\right) , \cos(\phi)\sin\left(\lambda + \omega_{Earth} t\right) , \sin(\phi)\right\}, \quad (4)$$

$$\vec{u}_\lambda(t) = \left\{-\sin\left(\lambda + \omega_{Earth} t\right) , \cos\left(\lambda + \omega_{Earth} t\right) , 0\right\}, \quad (5)$$

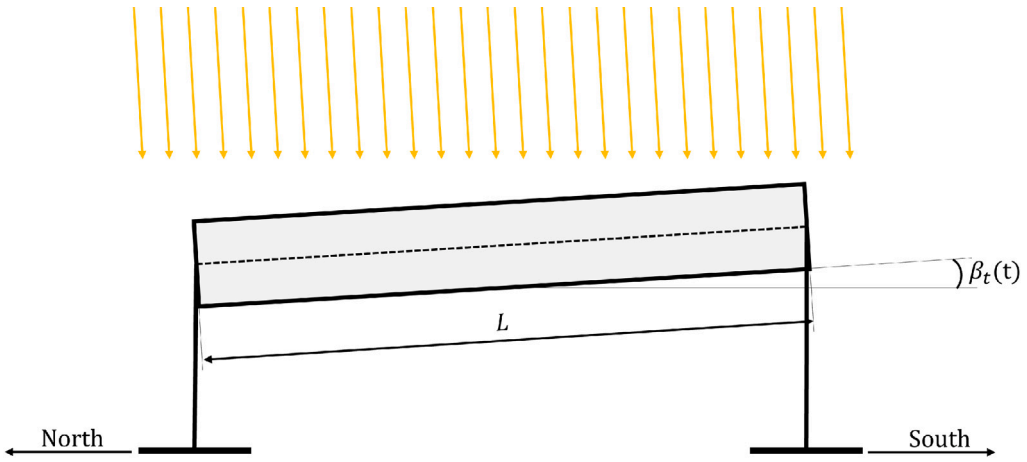

Fig. 2. Diagram illustrating the tilt angle of the solar panel or horizontally mounted solar tracker in the north–south direction (measured as positive towards the north), $\beta_t(t)$.

and

$$\vec{u}_\phi(t) = \left\{-\sin(\phi)\cos\left(\lambda + \omega_{Earth}t\right)\ , -\sin(\phi)\sin\left(\lambda + \omega_{Earth}t\right)\ , \cos(\phi)\right\}, \tag{6}$$

where $\omega_{Earth} = 2\pi/(24 \cdot 3600)$ rad/s is the angular velocity of Earth's rotation on itself.

From the previous expressions, the projections along each unit vector, radial, azimuthal, and polar, can be defined using the cosines formed by the unit vector in the direction of the Sun with each of the other three unit vectors:

$$\cos_i(t) = \vec{u}_{Sun}(t) \cdot \vec{u}_i(t) \quad \text{with} \quad i = r,\ \lambda \text{ or } \phi. \tag{7}$$

The previous expression is redefined so that, whenever the Sun is below the minimum solar elevation, ϵ_{min}, or above the maximum solar elevation, ϵ_{max}, imposed as input magnitudes, the projections are zero (assuming the Sun is below the horizon and, therefore, the area is not illuminated). Thus, it is defined as follows:

$$\cos_i(t) = \begin{cases} 0 \Leftrightarrow \left[\cos_\lambda(t) \geq \cos\left(\epsilon_{min}\right) \quad \text{or} \quad \cos_\lambda(t) \leq \cos\left(\epsilon_{max}\right)\right] \\ \qquad\qquad \text{or} \quad \cos_r(t) \leq 0 \\ \cos_i(t) \Leftrightarrow \left[\cos_\lambda(t) < \cos\left(\epsilon_{min}\right) \quad \text{and} \quad \cos_\lambda(t) > \cos\left(\epsilon_{max}\right)\right] \\ \qquad\qquad \text{and} \quad \cos_r(t) > 0 \end{cases}. \tag{8}$$

The previous expressions can be interpreted as the proportions of total incident solar irradiance, $\dot{Q}_T(t)$, from each region, such that $\dot{Q}_r(t)/\dot{Q}_T(t) = \cos_r(t)$, $\dot{Q}_\lambda(t)/\dot{Q}_T(t) = \cos_\lambda(t)$, and $\dot{Q}_\phi(t)/\dot{Q}_T(t) = \cos_\phi(t)$. Furthermore, it can be observed that $\dot{Q}_r(t)$ is always positive or zero. However, $\dot{Q}_\lambda(t)$ and $\dot{Q}_\phi(t)$ are positive when the Sun is incident from the east and north, respectively; and negative otherwise. Therefore, the previous expressions serve to measure the proportion of energy arriving from each direction, as well as to evaluate the direction from which this energy comes.

2.2. Orientation of photovoltaic panels according to their type

Once the directions of origin of the sun are known, depending on the type of solar panels, temporal laws are imposed for the tilt angle, $\beta_t(t)$, and seat angle, $\theta_t(t)$. Thus, the following is obtained:

- ***Fixed solar panels***:
  Since fixed solar panels are assumed, the inclination and tilt angles are determined by input magnitudes. The temporal laws are given by:

$$\beta_t(t) = \beta \quad \text{and} \quad \theta_t(t) = \theta. \tag{9}$$

- ***Single-axis east–west solar trackers***:

$$\beta_t(t) = \beta \quad \text{and} \quad \theta_t(t) = \theta_t^*(t) = \arcsin\left(\cos_\lambda(t)\right). \tag{10}$$

- ***Single-axis north–south solar trackers***:

$$\beta_t(t) = \beta_t^*(t) = \arcsin\left(\cos_\phi(t)\right) \quad \text{and} \quad \theta_t(t) = \theta. \tag{11}$$

- ***Dual-axis solar trackers***:

$$\beta_t(t) = \beta_t^*(t) = \arcsin\left(\cos_\phi(t)\right) \quad \text{and} \quad \theta_t(t) = \theta_t^*(t) = \arcsin\left(\cos_\lambda(t)\right). \tag{12}$$

2.3. Shadow factor

Once the orientation of PV panels, given by $\beta_t(t)$ and $\theta_t(t)$, is known, the shadow factor for solar trackers can be estimated (for fixed panels, a single row is considered, $N = 1$).

Considering that all rows are equispaced during periods of illumination, there is a single row that remains fully illuminated at all times. The remaining $N - 1$ rows are either all illuminated or all shaded by a certain area fraction, $F(t)$. A conceptual diagram of the considered layout is shown in Fig. 3. For a given PV panel chord and seat angle (W and $\theta_t(t)$, respectively), the spacing between rows, D, is related to the area fraction $F(t)$ as follows:

$$D\left|\cos\left(\theta_t(t)\right)\right| = W\left(1 - F(t)\right), \tag{13}$$

and simply dividing by W, we obtain:

$$\frac{D}{W}\left|\cos\left(\theta_t(t)\right)\right| = 1 - F(t). \tag{14}$$

From the previous expression, the shadow factor $F(t)$ can be solved:

$$F(t) = \max\left[1 - \frac{D}{W}\left|\cos\left(\theta_t(t)\right)\right|, 0\right], \tag{15}$$

where $F(t) \geq 0$ is imposed as a negative area fraction cannot be illuminated, nor greater than the total area of the solar panel. Additionally, the shadow that one panel casts on another during the first half of the day is equal to the shadow it subsequently receives.

2.4. Cell efficiency and packing factor

When analyzing the electrical performance of solar panels, these are assumed to be composed of PV cells with an efficiency η_{cell}, which quantifies the ratio of energy generated to the normal incident energy. All solar panels contain a fixed number of PV cells, which collectively occupy an area A_{cells} on each panel. To account for the effects of shading and cell spacing on electrical production, the configuration

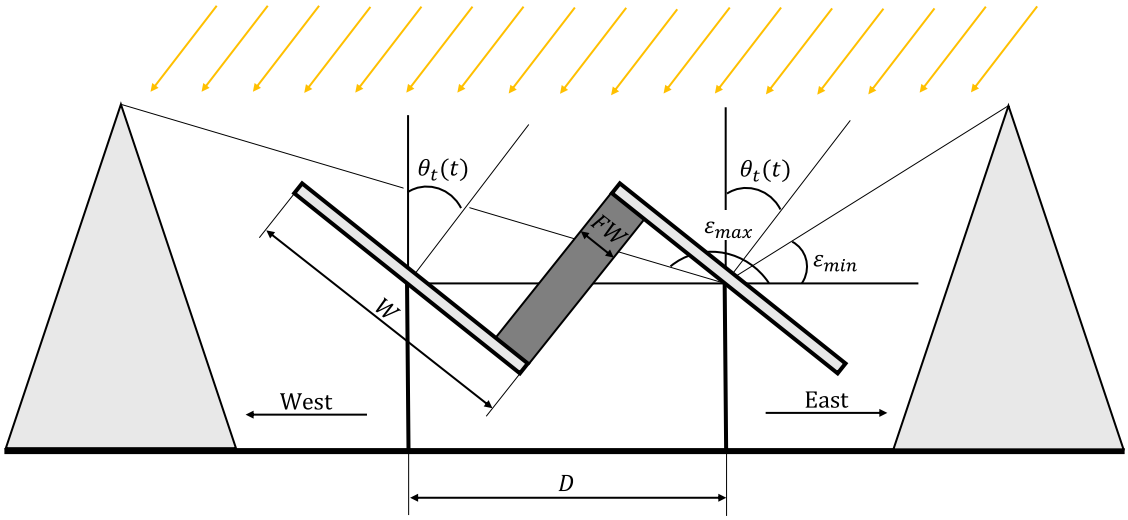

Fig. 3. Conceptual diagram of shadow appearance in solar trackers.

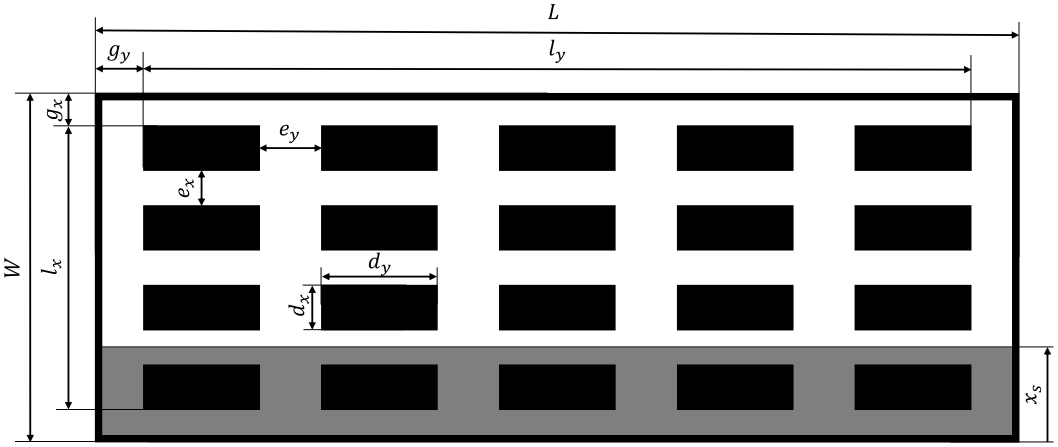

Fig. 4. Schematic representation of shadow effects on solar tracker cells.

depicted in Fig. 4 is considered. In this model, shading on any part of a solar cell causes the entire cell to cease energy generation. The PV cells are arranged in multiple rows aligned parallel to the span direction (*i.e.*, parallel to the rotation axis in the case of solar trackers). Consequently, when a single cell is shaded, all cells within the same row are likewise affected (see Fig. 4).

If the solar panel has N_x rows of cells aligned along the chord direction and N_y columns along the spanwise direction, the total area occupied by cells is given by $A_{cells} = N_x N_y d_x d_y$, where d_x and d_y represent the dimensions of an individual cell. Considering the dimensions illustrated in Fig. 4, the total area of the solar panel can be expressed as: $A_{panel} = LW = \left[N_x d_x + (N_x - 1)e_x + 2g_x\right]\left[N_y d_y + (N_y - 1)e_y + 2g_y\right]$, where e_x and e_y are the spacings between cells in the chord and spanwise directions, respectively, and g_x and g_y represent the edge gaps. Consequently, the packing factor η_{pack} can be expressed as:

$$\eta_{pack} = \frac{A_{cells}}{L\,W} = \frac{N_x N_y d_x d_y}{\left[N_x d_x + (N_x - 1)e_x + 2g_x\right]\left[N_y d_y + (N_y - 1)e_y + 2g_y\right]}. \tag{16}$$

The use of the packing factor η_{pack} implies an extension of the simple model depicted in Fig. 4 to a continuous one. When using it, it is assumed that if a fraction of the panel area is unshaded, $1 - F(t)$, the proportion of this unshaded area containing PV cells is given by η_{pack}. To assess the validity of this approximation compared to modeling the actual behavior of the solar panel, the following coefficient is defined:

$$\eta_F(t) = \frac{\text{Effective cells area}}{\text{Total panel area}} = \eta_{pack}\left[1 - F(t)\right]. \tag{17}$$

Fig. 5 illustrates the coefficient η_F as a function of the shading factor F and the seat angle θ, measured relative to the panel's normal. The coefficient is computed both exactly and using the continuous approximation. Based on the results shown in Fig. 5, the use of a constant packing factor and the neglecting of the detailed modeling of shading effects at the level of individual solar cells is justified. Accordingly, it is assumed that for a solar panel with shading factor F, the area fraction $\eta_{pack}(1 - F)$ contributes to energy production as a whole, disregarding the presence of partially shaded cells within this area.

2.5. Utilization efficiency

On the other hand, the surface utilization factor is defined as:

$$\eta_A = \frac{\text{Area occupied by solar panels}}{\text{Total area}} = \frac{N\,L\,W}{L\,W + (N-1)\,D\,L} = \frac{N}{1 + (N-1)\,D/W}. \tag{18}$$

Note that in the case of fixed solar panels, where $N = 1$, it holds that $\eta_A = 1$, meaning there is maximum utilization of the occupied area. From the previous expressions, a minimum value D/W^*_{min} can be

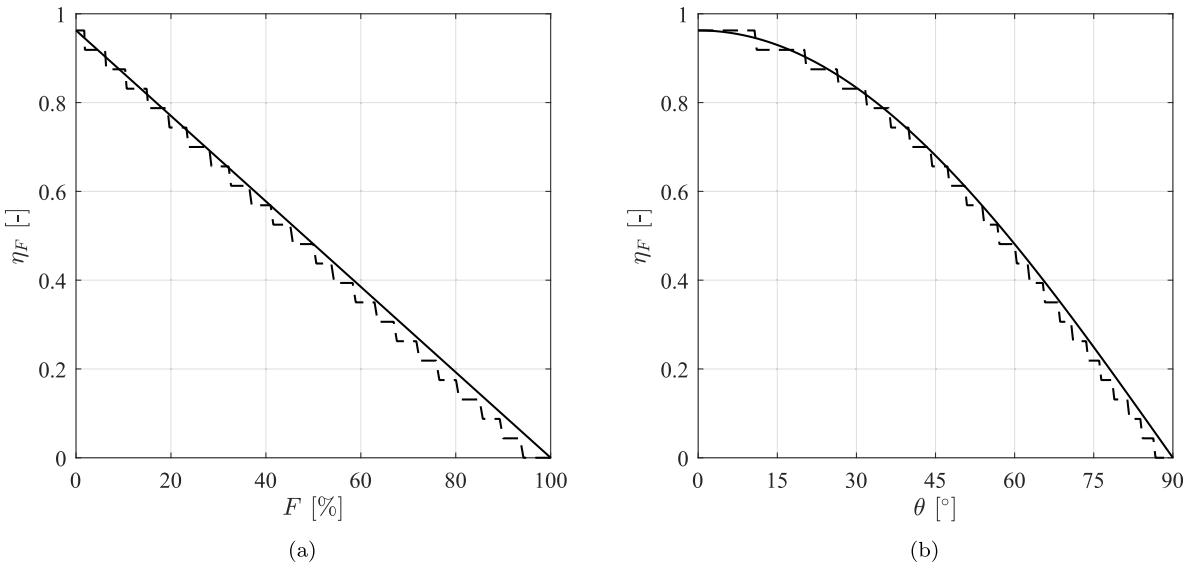

Fig. 5. Coefficient η_F obtained exactly (dashed line) and via the continuous approximation (solid line) as a function of the shading factor F (a) and the seat angle θ (b), considering the following values: $W = 4.8$ m, $d_x = d_y = 0.21$ m, $e_x = e_y = 0.0005$ m, and $g_x = g_y = 0.08475$ m.

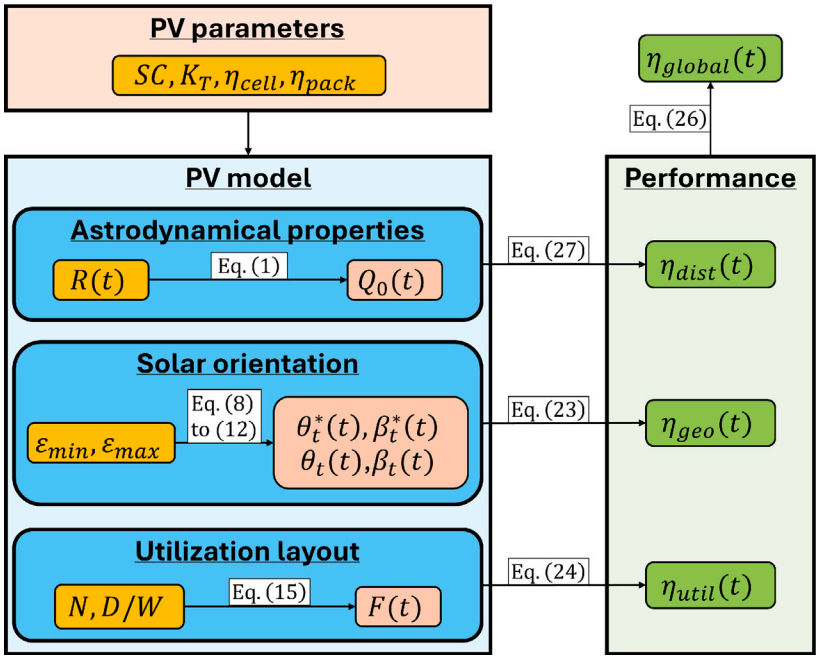

Fig. 6. Schematic representation of the functional relationships between the input variables (framed in blue) and the output variables (framed in green) through the indicated equations and the intermediate variables (framed in orange).

obtained, from which there is no shadow between the solar panels, *i.e.*, $F(t) = 0$. This minimum distance turns out to be:

$$D/W^*_{min} = \max\left[\frac{1}{\sin(\varepsilon_{min})}, \frac{1}{\sin(\varepsilon_{max})}\right]. \tag{19}$$

Likewise, for this value of D/W, a maximum value of the surface utilization factor allowing no shadow between the different rows of panels, $\eta^*_{A,max}$, arises. This value is computed as:

$$\eta^*_{A,max} = \min\left[\frac{N\sin(\varepsilon_{min})}{\sin(\varepsilon_{min}) + (N-1)}, \frac{N\sin(\varepsilon_{max})}{\sin(\varepsilon_{max}) + (N-1)}\right]. \tag{20}$$

When particularizing Eqs. (19) and (20) for the limit cases $\varepsilon_{min} = 0$ or $\varepsilon_{max} = \pi$, $D/W^*_{min} \to \infty$ and $\eta^*_{A,max} \to 0$.

2.6. Global efficiency

For the purposes of geometric and spatial distribution optimization, it is convenient to express the electrical power produced per unit of the total site area relative to the solar constant. This is achieved through the use of a global efficiency parameter, η_{global}, which accounts for all energy losses. Based on this framework, the electrical power output can be determined. Specifically, the first step involves calculating the solar power per unit area incident perpendicularly on any shadow-free solar panel (in the case of solar trackers, the one is typically located furthest east or west, depending on the time of day), obtained as:

$$\dot{q}_1(t) = \max\left[\dot{Q}_T(t)\cos\left(\theta_t(t) - \theta_t^*(t)\right)\cos\left(\beta_t(t) - \beta_t^*(t)\right), 0\right]. \tag{21}$$

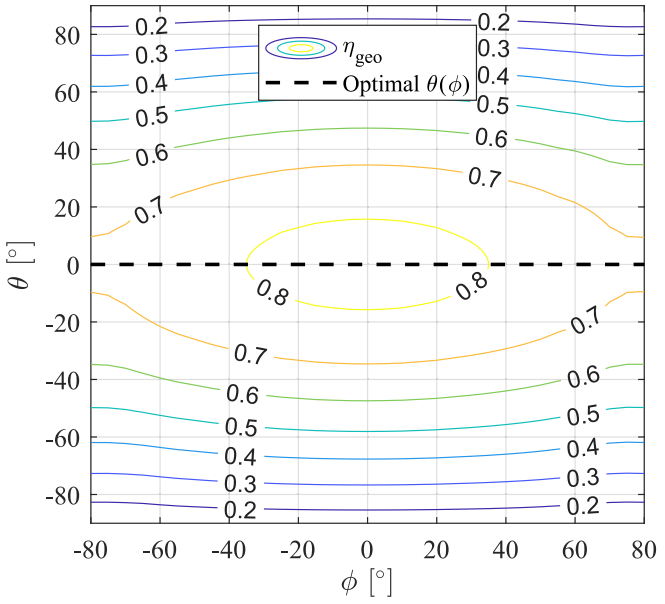

Fig. 7. Geometric efficiency contours, η_{geo}, as a function of the seat angle, θ, and the site's latitude, ϕ, assuming $\varepsilon_{min} = 0$ and $\varepsilon_{max} = \pi$.

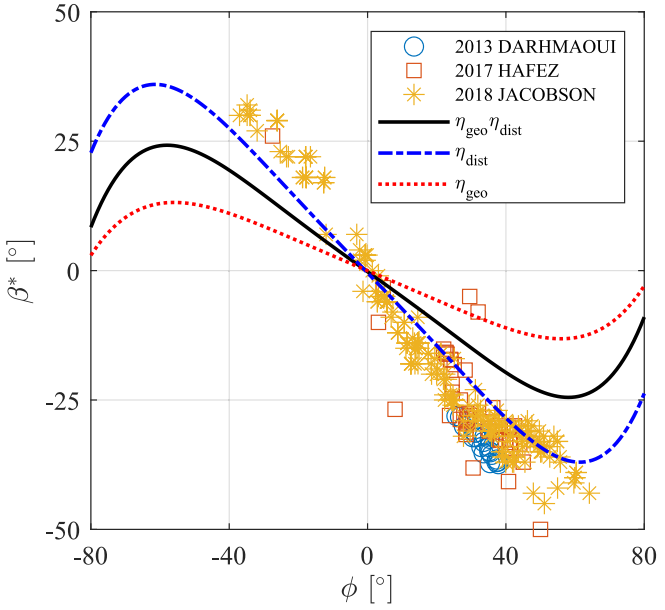

Fig. 8. Optimal tilt angle, β^*, as a function of the site's latitude, ϕ, optimizing $\eta_{dist}\eta_{geo}$ (black solid line), η_{geo} (blue dashed–dotted line), and η_{dist} (red dashed line). Results from Darhmaoui and Lahjouji [54] (○), Hafez et al. [56] (□), and Jacobson and Jadhav [57] (∗) are included.

From Eq. (21), the total power per unit global area, $A_{global} = LW + (N-1)\,DL$, incident on the solar panels is given by:

$$\dot{q}_{global}(t) = \eta_A \frac{1 + (N-1)\,(1 - F(t))}{N} \dot{q}_1(t). \tag{22}$$

Again, when considering a fixed solar panel, $N = 1$, it holds that $\dot{q}_{global}(t) \equiv \dot{q}_1(t)$. From Eq. (21), a geometric efficiency factor η_{geo} can be defined as:

$$\eta_{geo}(t) = \frac{\dot{q}_1(t)}{\dot{Q}_T(t)} = \max\left[\cos\left(\theta_t(t) - \theta_t^*(t)\right)\cos\left(\beta_t(t) - \beta_t^*(t)\right), 0\right]. \tag{23}$$

Likewise, a utilization efficiency, η_{util}, can be defined as follows:

$$\eta_{util}(t) = \frac{\dot{q}_{global}(t)}{\dot{q}_1(t)} = \eta_A \frac{1 + (N-1)\,(1 - F(t))}{N} = \frac{1 + (N-1)\,(1 - F(t))}{1 + (N-1)\,D/W} \tag{24}$$

Finally, from the energy reaching the solar panels, the packing factor η_{pack} and the efficiency of the solar cells η_{cell} must be taken into account to obtain the electric power produced. In addition, the total solar irradiance can be expressed in function of the extraterrestrial irradiance as $\dot{Q}_T(t) = K_T \dot{Q}_0(t)$. Thus, the global electric power, $\dot{q}_{global,elec}(t)$, produced per unit global area, A_{global}, turns out to be:

$$\dot{q}_{global,elec}(t) = K_T \eta_{cell} \eta_{pack} \eta_{geo}(t) \eta_{util}(t) \dot{Q}_0(t), \tag{25}$$

hence the global efficiency of the system at a certain time instant, t, $\eta_{global}(t)$, can be defined as:

$$\eta_{global}(t) = \frac{\dot{q}_{global,elec}(t)}{SC} = K_T \eta_{cell} \eta_{pack} \eta_{geo}(t) \eta_{util}(t) \eta_{dist}(t), \tag{26}$$

as well as its average, $\eta_{global} = \overline{\eta_{global}(t)}$, for which the time period taken must be specified (typically the entire time interval T, or only the period corresponding to the hours of illumination at the location where the solar panels are installed). In the above expression,

$$\eta_{dist}(t) = \dot{Q}_0(t)/SC \tag{27}$$

where $SC \simeq 1360$ W/m^2 is the solar constant. The above expressions can be integrated over a specific time interval, T, and multiplied by the global area, A_{global}, to obtain the electrical energy produced by the solar panels.

Once the theoretical formulation describing the electrical behavior of solar panels has been developed, an optimization process is undertaken. This process aims to achieve the maximum possible value of the global efficiency, η_{global}, within the considered time interval. Typically, the time interval considered is one year, although it may be beneficial to optimize for a specific time interval, for instance, if the energy produced will only be used for very specific purposes during particular seasons of the year. It can be noted that only the last three efficiencies (*i.e.*, $\eta_{geo}(t)$, $\eta_{util}(t)$, and $\eta_{dist}(t)$) contribute to the optimization, since the rest are constant. Fig. 6 shows the schematic representation of the functional relationships between the inputs and outputs variables of the model.

3. Geometrical optimization

In this section, the optimization of the design parameters is carried out by implementing the formulation developed in Section 2. A period of time of $T = 1$ year is considered, including therefore cyclic variations in the incoming solar radiation. It is assumed that the solar panels location is known (defined by λ and ϕ), as well as the minimum and maximum solar elevation angles, ε_{min} and ε_{max}; the chord and span of the solar panels, W and L; and the number of solar panel rows, N, or the available global area, A_{global}. Knowing the area, the number of tracker rows can be obtained as:

$$N = \text{floor}\left(1 + \frac{\frac{A_{global}}{L\,W} - 1}{\frac{D}{W}}\right). \tag{28}$$

Next, the values of θ^*, β^*, and D/W^* that optimize the production of electrical energy are analyzed, where * states for optimal value. To do this, each efficiency factor introduced in the previous section is optimized.

3.1. Optimization of geometric efficiency, η_{geo}

Regarding the geometric efficiency, $\eta_{geo}(t)$, it can be seen that it depends on the imposed laws for the seat angles, $\theta_t(t)$, and tilt angles, $\beta_t(t)$. If variable control laws are imposed on these angles, as in the case of dual-axis solar trackers, the geometric efficiency is always $\eta_{geo} = 1$ during periods of illumination, and zero otherwise. On the other hand, when using fixed solar panels or single-axis solar trackers, it is of interest to know the optimal value of the angles that remain fixed.

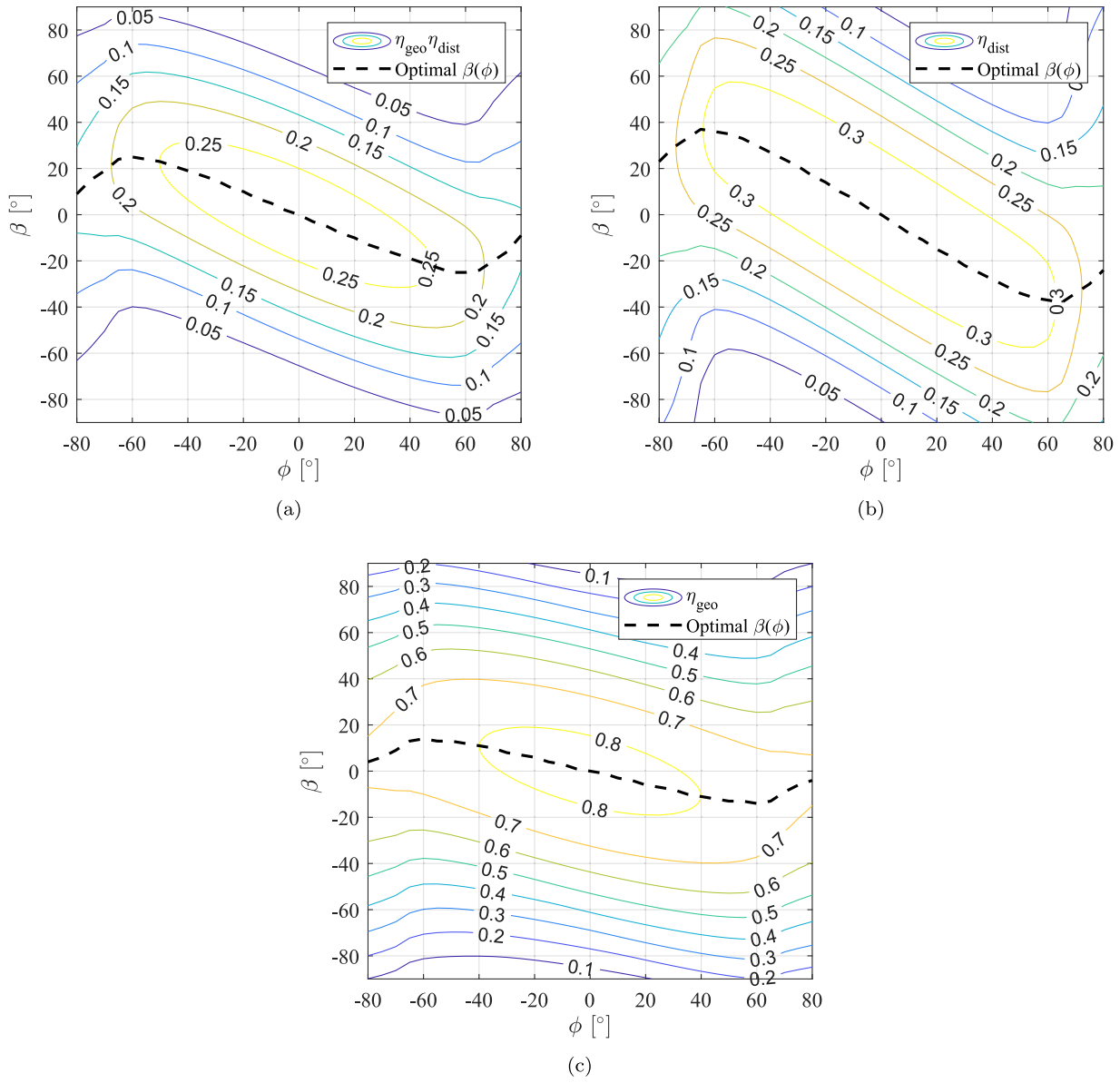

Fig. 9. Efficiency contours, $\eta_{dist}\eta_{geo}$ = const. (a), η_{dist} = const. (b), and η_{geo} = const. (c), as a function of the tilt angle, β, and the site's latitude, ϕ.

Since both angles are decoupled, they can be analyzed separately. For fixed solar panels and single-axis north–south trackers, the optimal seat angle, θ^*, is derived from purely geometric considerations. In particular, it is found that the optimal angle is:

$$\theta^* = \frac{\pi}{2} - \frac{\epsilon_{min} + \epsilon_{max}}{2}. \tag{29}$$

Two important conclusions are derived from Fig. 7 in which the contours for different constant values of η_{geo} as a function of latitude, ϕ, and the seat angle, θ, are depicted. First, η_{geo} decreases as the seat angle deviates from the optimal value (*i.e.*, $\theta^* = 0$ for the ϵ_{min} and ϵ_{max} values considered). Second, the optimal value of θ^* is not affected by the latitude.

Although the relative motion of the Sun and Earth can be neglected over a single day, this effect should be considered when optimizing the tilt angle on an annual basis. Consequently, three parameters can be optimized: $\eta_{dist}\eta_{geo}$, η_{geo}, and η_{dist}, which generally yield different values for the optimal tilt angle. Fig. 8 shows the optimal tilt angle, β^*, as a function of latitude, ϕ, for the three aforementioned optimizations. Results provided by Darhmaoui and Lahjouji [54], Hafez et al. [56], and Jacobson and Jadhav [57] are also included for comparison.

From Fig. 8, it can be observed that the results for η_{dist} more closely replicate the values reported in the literature across various latitudes. However, it is also evident that certain data points align with the curve obtained by optimizing η_{geo}. Nevertheless, the curve that truly maximizes energy capture is the one obtained by optimizing $\eta_{dist}\eta_{geo}$. Indeed, this curve takes intermediate values between the aforementioned curves as well as the values found in the available literature. Based on the curves observation, the optimal tilt angle as a function of latitude can be approximated by:

$$\beta^*(\phi) = C_0 + C_1\phi + C_2\phi^2 + C_3\phi^3 + C_4\phi^4 + C_5\phi^5, \tag{30}$$

where β^* and ϕ are expressed in radians, and the coefficients for optimizing $\eta_{dist}\eta_{geo}$, η_{dist}, and η_{geo} are given in Table 1.

In practice, various constraints may prevent setting solar panels at their optimal tilt angle. Therefore, understanding the sensitivity of performance to deviations in tilt angle and latitude is of interest. Fig. 9-(a) illustrates the contours for different constant values of $\eta_{dist}\eta_{geo}$ as a function of β and ϕ, where the geometric efficiency loss can be computed for each case. Similarly, Fig. 9-(b) and -(c) illustrate the contours for different constant values of η_{dist} and η_{geo}, respectively, as a function of β and ϕ.

Table 1
Optimal tilt angle coefficients as a function of latitude, in accordance with Eq. (30), obtained by optimizing $\eta_{dist}\eta_{geo}$, η_{dist}, and η_{geo}.

Optimized variable	C_0	C_1	C_2
$\eta_{dist}\eta_{geo}$	$-3.796 \cdot 10^{-3}$	$-4.796 \cdot 10^{-1}$	$+3.838 \cdot 10^{-3}$
η_{dist}	$-7.793 \cdot 10^{-3}$	$-6.932 \cdot 10^{-1}$	$-2.118 \cdot 10^{-3}$
η_{geo}	0	$-2.842 \cdot 10^{-1}$	0
Optimized variable	C_3	C_4	C_5
$\eta_{dist}\eta_{geo}$	$-8.838 \cdot 10^{-2}$	$-2.366 \cdot 10^{-3}$	$+1.430 \cdot 10^{-1}$
η_{dist}	$-8.655 \cdot 10^{-2}$	$+9.253 \cdot 10^{-4}$	$+1.503 \cdot 10^{-1}$
η_{geo}	$-2.119 \cdot 10^{-2}$	0	$+7.592 \cdot 10^{-2}$

Although the results presented thus far are all dimensionless and therefore universally applicable to any location regardless of its specific characteristics, it may be of interest to conduct comparisons based on a specific site. This would allow for the evaluation of both dimensionless and dimensional values. The comparison of dimensionless values has already been conducted, with a particular focus on optimal angles, as shown in Fig. 8. It should be noted that the results provided by Darhmaoui and Lahjouji [54], Hafez et al. [56], and Jacobson and Jadhav [57] originate from various authors who employ both experimental tests and mathematical models of varying complexity.

Regarding the comparison of dimensional values (such as data on generated electrical energy or solar radiation captured by a given surface), available information is limited. Even though the comprehensiveness of the model presented in this study enables the incorporation of multiple factors for determining the electrical power generated by PV solar panels, most references that conduct experimental tests provide data on electrical power generation without specifying the efficiency of the solar cells used or the packing factors. Consequently, the only values that can be directly compared with the model developed in this study are the optimal angles, which have already been included in the comparison made in Fig. 8. Moreover, references that do provide data on captured solar radiation often omit information on the prevailing solar irradiance at the time of data collection, making it difficult to determine the K_T factor.

Due to the scarcity of available results in the literature that consider all the factors included in our model, the replication of dimensional results becomes challenging. To facilitate a comparison of dimensional data, an illustrative example is provided using the data from Bruno et al. [61]. These authors provide data on both annual direct solar radiation and the solar radiation collected by a flat plate for different control laws and tilt angles, using Cosenza, Italy, as a reference location. Specifically, their study determines an annual optimal tilt angle of $-30°$ (*i.e.*, with the solar panel facing south), which is very close to the $-28°$ obtained using the model developed in this study when considering the tilt angle that maximizes η_{dist} for Cosenza's latitude. However, when optimizing for $\eta_{dist}\eta_{geo}$, the optimal tilt angle is found to be $-19°$. Moreover, assuming $K_T\eta_{cell}\eta_{pack} = 1$ in our model, the ratio of the total energy produced to the energy received from the Sun during the hours of solar illumination throughout the year (both considered under extraterrestrial conditions, assuming $K_T = 1$) is $\simeq 0.96$, regardless of whether the tilt angle is optimized for η_{dist} or for $\eta_{dist}\eta_{geo}$. In the case of the data provided by Bruno et al. [61], for the optimal tilt angle of $-30°$, the ratio of the beam solar radiation (2115 kWh/m^2) to the annual direct normal radiation (2194 kWh/m^2) is also approximately $2115/2194 \simeq 0.96$. Additionally, when assuming a factor of $K_T \approx 0.4$ (based on the direct normal radiation values reported by Bruno et al. [61]), the model developed in this study successfully reproduces the beam solar radiation obtained. This holds true regardless of whether the tilt angle is optimized for η_{dist} or for $\eta_{geo}\eta_{dist}$, with differences between the two cases remaining below 1%. The fact that, despite the approximately 10° difference in the optimum tilt angle when optimizing η_{dist} or $\eta_{dist}\eta_{geo}$, the predicted annual energy production is approximately the same, and also equal to the one predicted by Bruno et al. [61] is due to the low sensitivity of the tilt angle to changes near the optimum, as observed in the contours shown in Fig. 9.

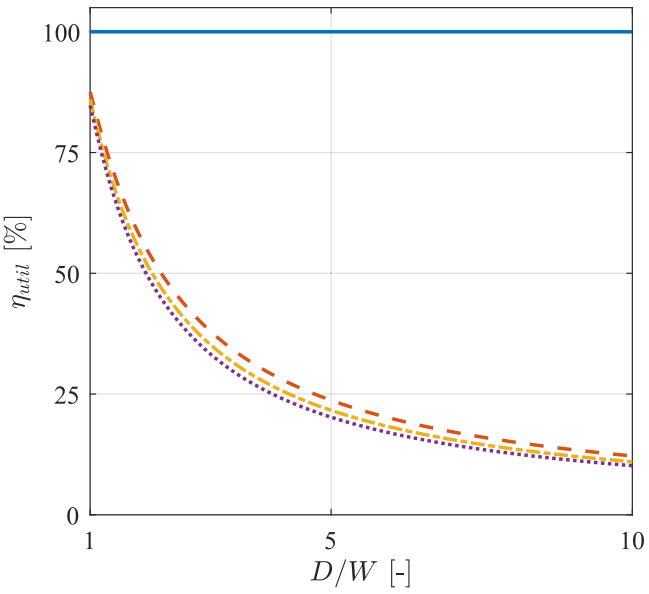

Fig. 10. Utilization efficiency, η_{util}, as a function of the dimensionless distance between rows, D/W, for $N = 1$ (blue solid line), 5 (orange dashed line), 10 (yellow dash-dotted line), and 50 (purple dotted line).

3.2. Optimization of utilization efficiency, η_{util}

For solar trackers, the maximization of the utilization efficiency $\eta_{util} = \overline{\eta_{util}(t)}$ requires determining the optimal dimensionless distance between trackers, D/W. Using Eqs. (24) and (28), $\eta_{util}(t)$ is expressed as:

$$\eta_{util}(t) = \frac{1 + \mathrm{floor}\left[\frac{W}{D}\left(\frac{A_{global}}{L\ W} - 1\right)\right][1 - F(t)]}{1 + \frac{A_{global}}{L\ W}}. \tag{31}$$

where $F(t)$, the shading factor, varies between $F = 0$ and $F = 1 - \frac{D}{W}|\cos(\theta_t(t))|$. Taking the above into account, the utilization efficiency takes the form:

$$\eta_{util}(t) = \frac{1 + \mathrm{floor}\left(\frac{A_{global}}{L\ W} - 1\right)\ |\cos(\theta_t(t))|}{1 + \frac{A_{global}}{L\ W}}, \tag{32}$$

which, when considering the optimal distance, gives:

$$\eta_{util} = \frac{1 + \mathrm{floor}\left(\frac{\frac{A_{global}}{L\ W} - 1}{\frac{D}{W}}\right)}{1 + \frac{A_{global}}{L\ W}}. \tag{33}$$

The efficiency loss due to increased distance is shown in Fig. 10 according to Eq. (33). Efficiency declines with increased D/W, but this decrease becomes asymptotic at larger distances. From this figure, the optimal distance is $D/W^* = 1$. However, practical considerations, such as maintenance and cleaning, often necessitate larger distances.

Fig. 11 presents the contours for different constant values of η_{util} as a function of D/W and N. It is evident that distance has a greater influence than the number of rows once $N > 2$. For $D/W > 2$, efficiency drops below 50% for $N > 10$, indicating the necessity of maintaining $D/W < 2$ whenever feasible.

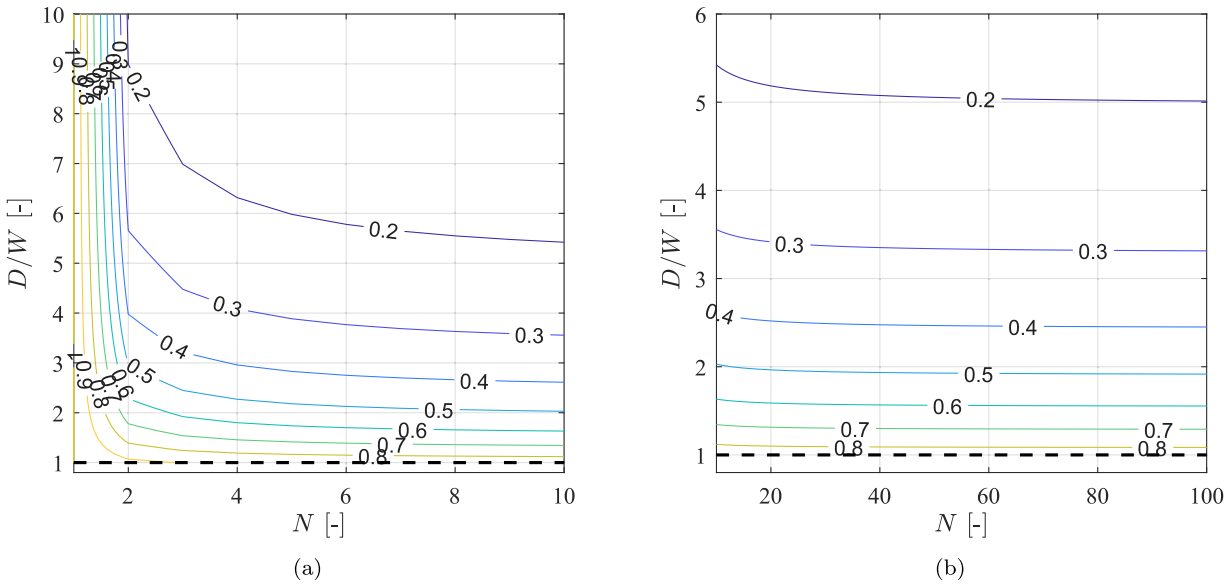

Fig. 11. Utilization efficiency contours (solid lines), η_{util}, as a function of the dimensionless distance between rows, D/W, and the number of rows, N, and optimal $D/W(N)$ curve (black dashed lines).

4. Conclusions

In this paper, a comprehensive review of the state of the art in solar radiation, PV energy production, and its optimization has been undertaken. A simplified mathematical model has been developed, which decouples the various factors influencing the electrical production of solar panels and provides a holistic view of PV energy production (see Fig. 6 for a schematic view of the developed mathematical model inputs and outputs). This model is applicable to both fixed systems and solar trackers. Furthermore, the implications of several commonly employed modeling assumptions have been evaluated. Notably, the hypothesis of neglecting the spacing between solar cells when accounting for shading effects has been analyzed. The analysis revealed that, for small cell sizes and inter-cell distances, a constant packing factor can be assumed, validating the approximation of the solar panel as a continuous medium. As a result, a formulation has been derived that represents the transformation of solar radiation into electrical energy through multiple efficiency factors.

Building on the developed mathematical model, this study explores the optimization of key parameters affecting the performance of solar panels and tracking systems, including the seat angle, tilt angle, and the dimensionless distance between rows (D/W). The findings provide important insights into geometric and utilization efficiencies, offering practical guidance for solar park design and operation.

Optimization of geometric efficiency (η_{geo}): The analysis of η_{geo} revealed that the seat angle has an optimal value, θ^*, that is independent of latitude. Deviations from this optimal value lead to significant decreases in geometric efficiency. Similarly, optimizing the tilt angle, β^*, demonstrated its dependence on latitude, with the derived polynomial approximation providing a practical tool for estimating the optimal tilt angle across diverse latitudes. A comparison of the optimal values predicted by the present model with those found in the literature shows good agreement, on average. Sensitivity analyses of η_{geo} contours as a function of latitude and tilt angle highlighted that small deviations around the optimal values result in moderate efficiency losses, while larger deviations lead to substantial impacts, underscoring the importance of precise alignment during installation.

Optimization of utilization efficiency (η_{util}): The study identified that the optimal dimensionless distance between rows, in terms of global power generation, is $D/W^* = 1$. However, practical considerations, such as the need for maintenance and cleaning, require larger distances. The associated efficiency losses were quantified, revealing an asymptotic decline in η_{util} for increasing D/W values, particularly for solar parks with a significant number of rows ($N > 10$).

Practical design implications: For efficient solar park design, maintaining $D/W < 2$ is crucial to avoiding significant utilization efficiency losses. The results further indicate that, beyond a certain number of rows, the influence of N becomes negligible compared to D/W, offering valuable insights for cost-efficient layout decisions in large-scale solar installations.

This comprehensive analysis provides both theoretical and practical contributions, offering a robust framework for optimizing solar tracker systems to maximize energy generation while accounting for real-world constraints. Regarding future research opportunities arising from this study, several key directions can be identified:

First, the developed mathematical model allows for both a dimensionless treatment, as applied in this article, and a dimensional approach, enabling the estimation of total energy production over a given period based on specific characteristics of the considered PV plant. In this regard, it would be valuable to compare the dimensional results obtained through this model with real-world data from actual PV plants, provided that their characteristics and site-specific conditions are well known.

Second, reviewing and improving the modeling of all factors influencing solar panel and solar tracker energy production, which intervene in Eq. (26), would be of significant interest. While existing models account for these effects, they are often highly complex. Therefore, refining the simplified model to achieve a more accurate representation of real-world conditions, while preserving its simplicity and general applicability, would be beneficial, as this aspect is often lacking in current models. For instance, the effect of temperature on cell efficiency, η_{cell}, could be incorporated in a simplified manner by modeling the convective cooling effect based on average values of wind speed, absorptance, and the convective coefficient of solar panels.

Third, in certain cases, it may be desirable to achieve a stable and uniform PV electricity production throughout the year by using multiple solar panels of varying sizes and orientations (*e.g.*, for residential applications where electricity consumption remains relatively constant over the year or a specific period). In such a scenario, the simplified mathematical model developed in this study could be used to determine the optimal angles for each solar panel that, while ensuring a production curve as uniform as possible (potentially evaluated through

merit figures assessing homogeneity over the considered time period), also maximize annual energy production.

These future research directions would further enhance the applicability and impact of the proposed model, bridging the gap between theoretical optimization and real-world implementation. Moreover, both the developed model and the potential advancements in future research lines contribute to improving the productivity of next-generation PV solar farms.

CRediT authorship contribution statement

Carlos Carbajosa: Writing – original draft, Validation, Software, Investigation, Formal analysis, Data curation, Conceptualization. **Sergio Marín-Coca:** Writing – review & editing, Supervision, Project administration, Methodology, Formal analysis, Conceptualization. **Miguel Gavira-Aladro:** Writing – review & editing, Validation, Software, Methodology, Formal analysis, Conceptualization. **Alejandro Martínez-Cava:** Writing – review & editing, Supervision, Resources, Project administration, Funding acquisition.

Declaration of Generative AI and AI-assisted technologies in the writing process

During the preparation of this work, the authors used ChatGPT in order to improve the translation and readability of the document. After using this tool, the authors reviewed and edited the content as needed and take full responsibility for the content of the published article.

Declaration of competing interest

The authors declare that they have no known competing financial interests or personal relationships that could have appeared to influence the work reported in this paper.

Acknowledgments

This work is part of the project TED2021-130541B-C21, funded by MCIN/AEI/10.13039/501100011033, the European Union "NextGenerationEU"/PRTR and project PID 2022-137630OB-C21 financed by MCIN/AEI/10.13039/501100011033/FEDER, UE. This research was supported by the FPU grant (Formación de Profesorado Universitario) FPU23/00716 from the Spanish Ministry of Science and Innovation (Ministerio de Ciencia, Innovación *y* Universidades) to Carlos Carbajosa and the FPU grant (Formación de Profesorado Universitario) FPU23/00509 from the Spanish Ministry of Science and Innovation (Ministerio de Ciencia, Innovación *y* Universidades) to Miguel Gavira-Aladro.

References

[1] IEA, World Energy Outlook 2022, International Energy Agency, 2022, p. 522, URL https://www.iea.org/reports/world-energy-outlook-2022.

[2] IRENA, Global Landscape of Renewable Energy Finance, International Renewable Energy Agency, 2023, p. 131, URL https://www.irena.org/Publications/2023/Feb/Global-landscape-of-renewable-energy-finance-2023.

[3] M. Sohail, H.N. Afrouzi, K. Mehranzamir, J. Ahmed, M.B. Mobin Siddique, M. Tabassum, A comprehensive scientometric analysis on hybrid renewable energy systems in developing regions of the world, Results Eng. 16 (2022) 100481, http://dx.doi.org/10.1016/j.rineng.2022.100481.

[4] E. Dupont, H. Koppelaar, H. Jeanmart, Global available solar energy under physical and energy return on investment constraints, Appl. Energy 257 (2020) http://dx.doi.org/10.1016/j.apenergy.2019.113968.

[5] M.K.H. Rabaia, Environmental impacts of solar energy systems: A review, Sci. Total Environ. 754 (2021) http://dx.doi.org/10.1016/j.scitotenv.2020.141989.

[6] S. Gorjian, H. Sharon, H. Ebadi, K. K., S.F. B., G.M. Tina, Recent technical advancements, economics and environmental impacts of floating photovoltaic solar energy conversion systems, J. Clean. Prod. 278 (2021) http://dx.doi.org/10.1016/j.jclepro.2020.124285.

[7] A. El Hammoumi, S. Chtita, S. Motahhir, A. El Ghzizal, Solar PV energy: From material to use, and the most commonly used techniques to maximize the power output of PV systems: A focus on solar trackers and floating solar panels, Energy Rep. 8 (2022) 11992–12010, http://dx.doi.org/10.1016/j.egyr.2022.09.054.

[8] K. Kumar, L. Varshney, A. Ambikapathy, R.K. Saket, S. Mekhilef, Solar tracker transcript—A review, Int. Trans. Electr. Energy Syst. 31 (12) (2021) e13250, http://dx.doi.org/10.1002/2050-7038.13250.

[9] A. Whillier, The determination of hourly values of total solar radiation from daily summations, Theor. Appl. Climatol. (1956) http://dx.doi.org/10.1007/bf02243322.

[10] A. Angstrom, Solar and terrestrial radiation. Report to the international commission for solar research on actinometric investigations of solar and atmospheric radiation, Q. J. R. Meteorol. Soc. 50 (210) (1924) 121–126, http://dx.doi.org/10.1002/qj.49705021008.

[11] G. Löf, G.O. Löf, J.A. Duffie, J.A. Duffie, C. Smith, C. Smith, World distribution of solar radiation, Sol. Energy (1966) http://dx.doi.org/10.1016/0038-092x(66)90069-7.

[12] J.N. Black, J.N. Black, The distribution of solar radiation over the earth's surface, Null (1956) http://dx.doi.org/10.1007/bf02243320.

[13] R. Swartman, R. Swartman, O. Ogunlade, O. Ogunlade, Solar radiation estimates from common parameters, Sol. Energy (1967) http://dx.doi.org/10.1016/0038-092x(67)90026-6.

[14] P. Moon, Proposed standard solar-radiation curves for engineering use, J. Frankl. Inst.- Eng. Appl. Math. (1940) http://dx.doi.org/10.1016/s0016-0032(40)90364-7.

[15] B.Y. Liu, R.C. Jordan, The interrelationship and characteristic distribution of direct, diffuse and total solar radiation, Sol. Energy (1960) http://dx.doi.org/10.1016/0038-092x(60)90062-1.

[16] B.Y.H. Liu, B.Y. Liu, R.C. Jordan, R.C. Jordan, The long-term average performance of flat-plate solar-energy collectors, Sol. Energy (1963) http://dx.doi.org/10.1016/0038-092x(63)90006-9.

[17] K.Y. Kondratyev, Radiation in the Atmosphere, first ed., vol. 12, Academic Press, 1969, p. 911.

[18] S.E. Tuller, S.E. Tuller, The relationship between diffuse, total and extra terrestrial solar radiation, Sol. Energy (1976) http://dx.doi.org/10.1016/0038-092x(76)90025-6.

[19] J.E. Hay, J.E. Hay, A revised method for determining the direct and diffuse components of the total short2010wave radiation, Atmos. (1976) http://dx.doi.org/10.1080/00046973.1976.9648423.

[20] J. Orgill, J.F. Orgill, K. Hollands, K. Hollands, Correlation equation for hourly diffuse radiation on a horizontal surface, Sol. Energy (1977) http://dx.doi.org/10.1016/0038-092x(77)90006-8.

[21] S. Klein, S. Klein, Calculation of monthly average insolation on tilted surfaces, Sol. Energy (1977) http://dx.doi.org/10.1016/0038-092x(77)90001-9.

[22] D. Ruth, D. Ruth, R.E. Chant, R. Chant, The relationship of diffuse radiation to total radiation in Canada, Sol. Energy (1976) http://dx.doi.org/10.1016/0038-092x(76)90049-9.

[23] R. Bruno, R. Bruno, A correction procedure for separating direct and diffuse insolation on a horizontal surface, Sol. Energy (1978) http://dx.doi.org/10.1016/0038-092x(78)90148-2.

[24] P.W. Suckling, P. Suckling, J.E. Hay, J.E. Hay, A cloud layer-sunshine model for estimating direct, diffuse and total solar radiation, Atmos. (1977) http://dx.doi.org/10.1080/00046973.1977.9648441.

[25] D.T. Reindl, D.T. Reindl, W. Beckman, W.A. Beckman, J.A. Duffie, J.A. Duffie, Diffuse fraction correlations, Sol. Energy (1990) http://dx.doi.org/10.1016/0038-092x(90)90060-p.

[26] D. Erbs, D. Erbs, S. Klein, S. Klein, J.A. Duffie, J.A. Duffie, Estimation of the diffuse radiation fraction for hourly, daily and monthly-average global radiation, Sol. Energy (1982) http://dx.doi.org/10.1016/0038-092x(82)90302-4.

[27] J. Spencer, J. Spencer, A comparison of methods for estimating hourly diffuse solar radiation from global solar radiation, Sol. Energy (1982) http://dx.doi.org/10.1016/0038-092x(82)90277-8.

[28] K. Hollands, K. Hollands, R. Huget, R. Huget, A probability density function for the clearness index, with applications, Sol. Energy (1983) http://dx.doi.org/10.1016/0038-092x(83)90149-4.

[29] J.E. Hay, J.E. Hay, Calculation of monthly mean solar radiation for horizontal and inclined surfaces, Sol. Energy (1979) http://dx.doi.org/10.1016/0038-092x(79)90123-3.

[30] P. Bendt, P. Bendt, M. Collares-Pereira, M. Collares-Pereira, A. Rabl, A. Rabl, A. Rabl, The frequency distribution of daily insolation values, Sol. Energy (1981) http://dx.doi.org/10.1016/0038-092x(81)90013-x.

[31] C. Gueymard, Critical analysis and performance assessment of clear sky solar irradiance models using theoretical and measured data, Sol. Energy 51 (2) (1993) 121–138, http://dx.doi.org/10.1016/0038-092X(93)90074-X.

[32] J. Davies, J.A. Davies, W.M. Schertzer, W. Schertzer, M.N. nez, M. Nuñez, M. Nunez, Estimating global solar radiation, Bound.-Layer Meteorol. (1975) http://dx.doi.org/10.1007/bf00232252.

[33] D. Norris, D. Norris, Correlation of solar radiation with clouds, Sol. Energy (1968) http://dx.doi.org/10.1016/0038-092x(68)90029-7.

[34] A. Whillier, Solar Energy Collection and Its Utilization for House Heating (Ph.D. thesis), Massachusetts Institute of Technology. Dept. of Mechanical Engineering, 1953, URL https://dspace.mit.edu/handle/1721.1/11922.
[35] A. Durgadevi, S. Arulselvi, S. Natarajan, Photovoltaic modeling and its characteristics, in: 2011 International Conference on Emerging Trends in Electrical and Computer Technology, 2011, pp. 469–475, http://dx.doi.org/10.1109/ICETECT.2011.5760162.
[36] A.R. Jordehi, Parameter estimation of solar photovoltaic (PV) cells: A review, Renew. Sustain. Energy Rev. 61 (2016) 354–371, http://dx.doi.org/10.1016/j.rser.2016.03.049.
[37] L. El Chaar, L. lamont, N. El Zein, Review of photovoltaic technologies, Renew. Sustain. Energy Rev. 15 (5) (2011) 2165–2175, http://dx.doi.org/10.1016/j.rser.2011.01.004.
[38] A.M. Oni, A.S.M. Mohsin, M.M. Rahman, M.B. Hossain Bhuian, A comprehensive evaluation of solar cell technologies, associated loss mechanisms, and efficiency enhancement strategies for photovoltaic cells, Energy Rep. 11 (2024) 3345–3366.
[39] C.M. Nkinyam, C.O. Ujah, K.C. Nnakwo, D.V.V. Kallon, Insight into organic photovoltaic cell: Prospect and challenges, Unconv. Resour. 5 (100121) (2025) 100121.
[40] K. Moradi, M. Ali Ebadian, C.-X. Lin, A review of PV/T technologies: Effects of control parameters, Int. J. Heat Mass Transfer 64 (2013) 483–500, http://dx.doi.org/10.1016/j.ijheatmasstransfer.2013.04.044.
[41] P. Yousefian, M. Durali, B. Rashidian, M.A. Jalali, Fabrication, characterization, and error mitigation of non-flat sun sensor, Sensors Actuators A: Phys. 261 (2017) 243–251, http://dx.doi.org/10.1016/j.sna.2017.05.022.
[42] S. Dubey, J.N. Sarvaiya, B. Seshadri, Temperature dependent photovoltaic (PV) efficiency and its effect on pv production in the world – a review, Energy Procedia 33 (2013) 311–321, http://dx.doi.org/10.1016/j.egypro.2013.05.072, PV Asia Pacific Conference 2012.
[43] A. Shukla, K. Kant, A. Sharma, P.H. Biwole, Cooling methodologies of photovoltaic module for enhancing electrical efficiency: A review, Sol. Energy Mater. Sol. Cells 160 (2017) 275–286, http://dx.doi.org/10.1016/j.solmat.2016.10.047.
[44] J.A. Cárdenas-Rondón, M. Ogueta-Gutiérrez, S. Franchini, R. Manzanares-Bercial, Stability analysis of two-dimensional flat solar trackers using aerodynamic derivatives at different heights above ground, J. Wind Eng. Ind. Aerodyn. 243 (2023) 105606, http://dx.doi.org/10.1016/j.jweia.2023.105606.
[45] J.A. Cárdenas-Rondón, C. Carbajosa, S. Marín-Coca, A. Martínez-Cava, Parametric analysis of self-excited aeroelastic instability of an isolated single-axis two-dimensional flat solar tracker, Results Eng. 24 (2024) 103539, http://dx.doi.org/10.1016/j.rineng.2024.103539.
[46] E. Díaz-Dorado, A. Suárez-García, C.J. Carrillo, J. Cidrás, Optimal distribution for photovoltaic solar trackers to minimize power losses caused by shadows, Renew. Energy 36 (6) (2011) 1826–1835, http://dx.doi.org/10.1016/j.renene.2010.12.002.
[47] N. ur Rehman, M. Uzair, Optimizing the inclined field for solar photovoltaic arrays, Renew. Energy 153 (2020) 280–289, http://dx.doi.org/10.1016/j.renene.2020.02.028.
[48] P. Subhashini, P. Chitra, N. Muthuvairavan Pillai, M. Vanitha, Theoretical enhancement of energy production performance in PV arrays through effective shadow detection using hybrid technique, Sol. Energy 264 (2023) 112006, http://dx.doi.org/10.1016/j.solener.2023.112006.
[49] B. He, H. Lu, C. Zheng, Y. Wang, Characteristics and cleaning methods of dust deposition on solar photovoltaic modules-a review, Energy 263 (2023) 126083, http://dx.doi.org/10.1016/j.energy.2022.126083.
[50] A. Phinikarides, N. Kindyni, G. Makrides, G.E. Georghiou, Review of photovoltaic degradation rate methodologies, Renew. Sustain. Energy Rev. 40 (2014) 143–152, http://dx.doi.org/10.1016/j.rser.2014.07.155.
[51] J. Kern, I. Harris, On the optimum tilt of a solar collector, Sol. Energy 17 (2) (1975) 97–102, http://dx.doi.org/10.1016/0038-092X(75)90064-X.
[52] K. Ulgen, Optimum tilt angle for solar collectors, Energy Sour. Part A: Recover. Util. Environ. Eff. 28 (13) (2006) 1171–1180, http://dx.doi.org/10.1080/00908310600584524.
[53] E. Mehleri, P. Zervas, H. Sarimveis, J. Palyvos, N. Markatos, Determination of the optimal tilt angle and orientation for solar photovoltaic arrays, Renew. Energy 35 (11) (2010) 2468–2475, http://dx.doi.org/10.1016/j.renene.2010.03.006.
[54] H. Darhmaoui, D. Lahjouji, Latitude based model for tilt angle optimization for solar collectors in the Mediterranean region, Energy Procedia 42 (2013) 426–435, http://dx.doi.org/10.1016/j.egypro.2013.11.043, Mediterranean Green Energy Forum 2013: Proceedings of an International Conference MGEF-13.
[55] A.K. Yadav, S. Chandel, Tilt angle optimization to maximize incident solar radiation: A review, Renew. Sustain. Energy Rev. 23 (2013) 503–513, http://dx.doi.org/10.1016/j.rser.2013.02.027.
[56] A. Hafez, A. Soliman, K. El-Metwally, I. Ismail, Tilt and azimuth angles in solar energy applications – a review, Renew. Sustain. Energy Rev. 77 (2017) 147–168, http://dx.doi.org/10.1016/j.rser.2017.03.131.
[57] M.Z. Jacobson, V. Jadhav, World estimates of PV optimal tilt angles and ratios of sunlight incident upon tilted and tracked PV panels relative to horizontal panels, Sol. Energy 169 (2018) 55–66, http://dx.doi.org/10.1016/j.solener.2018.04.030.
[58] A. Bahrami, C.O. Okoye, U. Atikol, The effect of latitude on the performance of different solar trackers in Europe and Africa, Appl. Energy 177 (2016) 896–906, http://dx.doi.org/10.1016/j.apenergy.2016.05.103.
[59] S. Frizzo Stefenon, C. Kasburg, A. Nied, A.C. Rodrigues Klaar, F.C. Silva Ferreira, N. Waldrigues Branco, Hybrid deep learning for power generation forecasting in active solar trackers, IET Gener. Transm. Distrib. 14 (23) (2020) 5667–5674, http://dx.doi.org/10.1049/iet-gtd.2020.0814.
[60] X. Chen, Y. Li, B. Zhao, R. Wang, Are the optimum angles of photovoltaic systems so important? Renew. Sustain. Energy Rev. 124 (2020) 109791, http://dx.doi.org/10.1016/j.rser.2020.109791.
[61] R. Bruno, P. Bevilacqua, L. Longo, N. Arcuri, Small size single-axis PV trackers: Control strategies and system layout for energy optimization, Energy Procedia 82 (2015) 737–743, http://dx.doi.org/10.1016/j.egypro.2015.11.802, 70th Conference of the Italian Thermal Machines Engineering Association, ATI2015.